Determination of Stack Plume Properties from Satellite Imagery

W. Frank Staylor*
NASA Langley Research Center, Hampton, Va.

LANDSAT imagery data were analyzed to determine the quantitative properties of a stack plume emitted from a moderate-sized pulp mill. Overlapping, consecutive-day multispectral scanner subsystem (MSS) data provided plume/no-plume radiances upwelling from the area of interest. These values from both the plume and its shadow were used to evaluate plume radius, height, particle concentration and scattering function, and total particle loading. Imagery data from a 10- by 10-km region in the vicinity of the mill were normalized to correct for minor atmospheric, solar, and viewing angle changes for the two observation days, and cloud shadow data were used to evaluate sky radiance. The effects of the sun angle, surface reflectance, signal-to-noise ratio (SNR), and spatial resolution are treated in the paper.

Introduction

THE dispersion of large smoke plumes from single and grouped stacks has been observed in LANDSAT imagery photoprints more than 100-km downwind from the stack sources.[1,2] Several studies have assumed that the measured increase in radiance above a plume is directly related to the columnar loading and have used these values to estimate plume parameters such as total loading, fallout, diffusion, and surface concentrations at downwind locations.[2,3] While these estimates may be adequate in some cases and for some uses, they can also be greatly in error. First of all, the plume radiance was determined by suppressing the apparent background radiance which is composed of both atmospheric backscattered and surface reflected radiances. The atmospheric radiance can be assumed constant across the plume, but the surface reflectance below the plume can vary considerably. Also, the plume shadowing effect was ignored, which can be a major radiance factor in the near-stack region. And, finally, the assumption that the plume radiance is directly related to the columnar loading is valid only if the size distribution of particles remains constant, which is generally not the case particularly in the near-stack region.

In the present paper, consecutive-day LANDSAT multispectral scanner subsystem (MSS) imagery data were obtained for a moderate-sized pulp mill site. The surface winds were blowing in different directions during the two orbital passes, and, therefore, plume/no-plume radiances were measured for the two days, permitting a relatively detailed analysis of the plume phenomena to be performed. Data from all four MSS spectral bands were utilized, allowing the wavelength dependence and, hence, the particle size distributions and mass loadings of the plumes to be determined. It is believed that the present analysis technique could provide quantitative plume properties that, when combined with ground measurements, meteorological data, and dispersion models, would offer a comprehensive program for monitoring industrial aerosols.

LANDSAT/MSS

The LANDSAT I spacecraft was inserted into a near-circular orbit at an altitude of 920 km with an inclination of 99 deg. This is a sun-synchronous orbit that passes over Virginia at about 9:30 a.m. on its descending node. The spacecraft has an MSS that images a 185-km swath of the Earth in four spectral bands (band 4, 0.5-0.6 μ; band 5, 0.6-0.7 μ; band 6, 0.7-0.8μ; band 7, 0.8-1.1μ).[4]

The LANDSAT orbit and MSS were designed to image the entire Earth between the 81 deg latitudes with an 18-day repeat cycle. As seen in Fig. 1, this results in imagery overlap on consecutive days which ranges from about 25 km at the Equator to 80 km at 50-deg latitude. Imagery data from an overlapped area were used in the present study because there is little change in the solar zenith and azimuth angles, and little probability of a significant surface reflectance change in one day compared to 18 days.

Stack Site

The site chosen to demonstrate the present analysis technique is a pulp mill located in West Point, Va., which is about 70-km east of Richmond, Va., at the conjunction of the Pamunkey and Mattaponi Rivers with the York River as shown in Fig. 2. The mill is primarily coal-fired, but also utilizes waste materials such as bark and sap as supplemental fuels. This particular plant stack was chosen because: 1) it emits only moderate quantities of smoke, and thus demonstrates that the present technique is not limited to major sources; 2) there are no other smoke-emitting plants in the immediate area, thus simplifying the analysis; and 3) it was in a region of LANDSAT MSS consecutive-day overlap. The MSS data employed in the present paper were obtained during orbital passes on Oct. 10 and 11, 1972, hereafter referred to as day 1 and day 2, respectively.

Normalization and Correction of the Measured Radiances

Radiances measured by the MSS on different days must first be normalized to conditions existing at the site during one

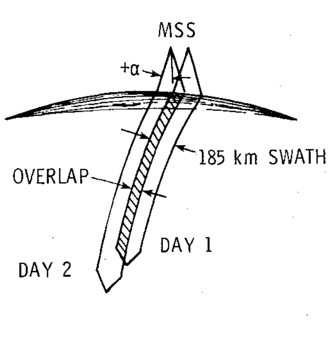

Fig. 1 LANDSAT MSS overlap.

Presented as Paper 77-72 at the AIAA 15th Aerospace Sciences Meeting, Los Angeles, Calif., Jan. 24-26, 1977; submitted Feb. 18, 1977; revision received Dec. 5, 1977. Copyright © American Institute of Aeronautics and Astronautics, Inc., 1977. All rights reserved.

Index category: Atmospheric and Space Sciences.

*Aerospace Technologist, Marine and Applications Technology Division. MemberAIAA.

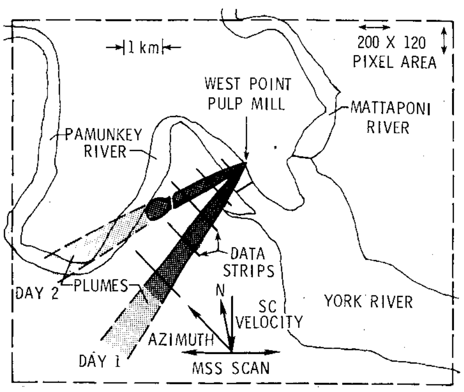

Fig. 2 Stack site and registered area.

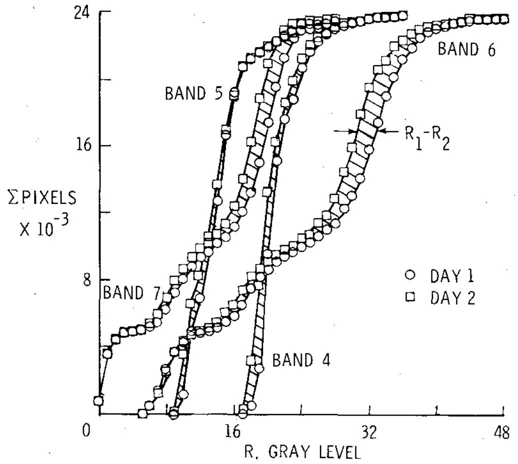

Fig. 3 Radiance corrections for stack site.

of the days, day 1 in this paper, in order to account for any differences in solar zenith and azimuth angles, nadir scan angle, atmosphere, or surface reflectance that may occur between the two days. Once the measured radiances have been normalized to a reference day, the atmospheric radiance for that day must be determined for the site and subtracted from the measured values in order that plume/no plume radiances can be observed without atmospheric contamination.

Measured radiances were normalized for a 200 by 120 pixel registered area centered about the pulp mill stack as shown in Fig. 2 (enclosed broken line area, ~10 by 10 km). The cumulative sum of pixels in the area having a measured radiance R or less (in gray levels) are plotted in Fig. 3 for all four spectral bands. Differences in the radiance levels between days 1 and 2, R_1-R_2, are the quantities that must be added to the R_2 values to normalize them to the reference day 1 conditions. Bands 4 and 5 (0.5 to 0.7 μ) require only 0 or 1 gray levels of correction, while bands 6 and 7 (0.7 to 1.1 μ) require 0 to 3 levels. The apparent reason for this difference in correction levels required to normalize the shorter and longer wavelength bands can be explained with the use of several basic relationships that will also be useful in later discussions. Table 1 gives geometrical and meteorological information that will be helpful in simplifying expressions and discussing the results.

The measured radiance R can be expressed as

$$R=\bar{R}+R_{\text{atm}} \tag{1}$$

where $\bar{R}$ is the scene radiance and R_{atm} is the upwelling atmospheric radiance.

$$\bar{R} \simeq \rho \cos\alpha I \tau^{\sec\alpha} \quad \text{for small } \alpha \tag{2}$$

Table 1 Geometrical and meteorological conditions

	Day 1	Day 2
Date	10/10/72	10/11/72
Time	9:30 a.m.	9:30 a.m.
Scan angle, α	+5.4 deg	−2.6 deg
Azimuth angle	146.6 deg	146.8 deg
Zenith angle, θ	49.9 deg	50.2 deg
Wind velocity, V	15 knots	9 knots
Wind direction	47 deg	72 deg
Relative humidity	50%	70%
No measurable rainfall since 10/7/72		

where ρ is the scene reflectance, α the nadir scan angle, I the solar irradiance at the scene, and τ is the atmospheric transmission. From Table 1, we find that cos α and sec $\alpha \approx 1$, and therefore,

$$\bar{R} \approx \rho I \tau \tag{3}$$

The scene irradiance can be expressed as

$$I=I_0 \cos\theta \tau^{\sec\theta}+I_{\text{sky}} \tag{4}$$

where I_0 is the solar irradiance above the atmosphere, θ is solar zenith angle, and I_{sky} is the downwelling sky irradiance. Substituting Eqs. (3) and (4) into Eq. (1) gives the relationship

$$R=\rho I_0 \cos\theta\left[\tau^{1+\sec\theta}+\frac{I_{\text{sky}}\tau}{I_0\cos\theta}\right]+R_{\text{atm}} \tag{5}$$

In Table 1, we find that $\theta_1 \approx \theta_2$, and as there is no reason to expect any significant changes of scene reflectance between day 1 and 2, we shall assume $\rho_1 \approx \rho_2$. The difference in the measured radiance between day 1 and 2 can now be expressed as

$$R_1-R_2 \approx \rho I_0 \cos\theta\left[\tau_1^{1+\sec\theta}-\tau_2^{1+\sec\theta}\right.$$
$$\left.+\frac{(I_{\text{sky}}\tau)_1-(I_{\text{sky}}\tau)_2}{I_0\cos\theta}\right]+R_{\text{atm}_1}-R_{\text{atm}_2} \tag{6}$$

A cursory study of Eq. (6) and Fig. 3 reveals that significant values of R_1-R_2 must be a result of a decrease in the atmospheric transmission on day 2, but only for bands 6 and 7. Water vapor absorbs strongly in bands 6 and 7 (0.7 to 1.1 μ), but not at all in bands 4 and 5 (0.5 to 0.7μ). Apparently, the water vapor content in the atmosphere was greater for day 2 which is supported by the ground measurement of relative humidity given in Table 1.

The atmospheric radiance, R_{atm}, could be measured directly over a spectrally black scene [i.e., $\rho=0$, see Eq. (5)], but rarely, if ever, do such ideal scenes exist in the natural environment. However, measurements from several sunlit/sun-shadowed scenes of differing reflectivities can be extrapolated to this ideal condition. With the assumption that $\tau_{\text{shadow}} \approx 0$ and $(R_{\text{atm}})_{\text{sun}} \approx (R_{\text{atm}})_{\text{shadow}}$, the radiance difference between a sunlit and sun-shadowed scene can be expressed as

$$R_{\text{sun}}-R_{\text{shadow}} \approx \rho I_0 \cos\theta\left[\tau_{\text{sun}}^{1+\sec\theta}\right.$$
$$\left.+\frac{(I_{\text{sky}}\tau)_{\text{sun}}-(I_{\text{sky}}\tau)'}{I_0\cos\theta}\right] \tag{7}$$

where $(I_{\text{sky}}\tau)'$ is the portion of sky radiance that is not occulted during the shadowing process.

Sunlit (day 2) and cloud-shadowed (day 1) radiances obtained for water, sand, field, and forest scenes located in the

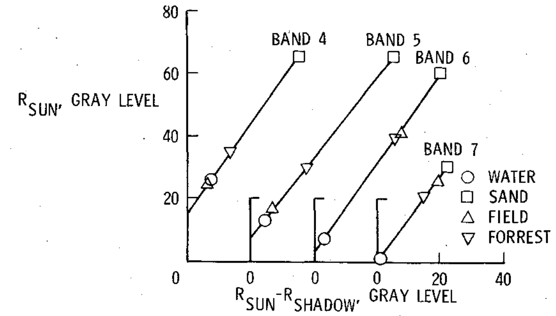

Fig. 4 Atmospheric radiance corrections.

York River area are presented in Fig. 4. Extrapolation of the $R_{\text{sun}} - R_{\text{shadow}}$ values to a zero value implies that $\rho = 0$ [i.e., spectrally black, see Eq. (7)] and at this point $R_{\text{sun}} = R_{\text{atm}}$ [see Eq. (5)]. The R_{atm} values obtained by this procedure are 15, 7, 3, and 1 gray levels for bands 4 through 7, respectively, which compare favorably with those given in Ref. 5 (central Michigan, Sept. 28, 1972). These atmospheric radiance values were subtracted from all normalized, measured radiances leaving the desired scene radiances [see Eq. (1)], which are free, in principle, of all solar, geometric, and atmospheric effects. In subsequent discussions, only normalized scene radiances $\bar{R}$ are used.

Analytical Plume Model

The present analytical model was derived specifically to utilize LANDSAT MSS measurements to determine the properties of stack plumes. The following assumptions are used in this model.

1) Gaussian particle distribution: $C = C_0 \exp[-\frac{1}{2}(r/r_0)^2]$
2) Plume locally cylindrical, high above surface: $G^{+\infty}_{-z_0} \approx 1$
3) Single scattering and small optical depth: $e^{-\beta} \approx 1 - \beta$
4) Lambertian surface reflection: $\rho_\theta = \rho_0 \cos\theta$
5) Small nadir scan angle: $\cos\alpha \approx 1$
6) Spectral dependence of particle scattering given by: λ^{-N}
7) Scattering function approximated by: $[\sin(\phi_0 + \phi)/2]^{-M}$
8) The particle absorption is approximately that for coal soot

Plume radiance $\bar{R}_P$ can be conveniently divided into three components illustrated in Fig. 5. The upward scattered radiance $\bar{R}_{US}$ is the product of 1) transmission (wavy line) of solar irradiance along ray to scattering volume, 2) vertical scattering by volume, and 3) vertical transmission from volume. Forward scattered radiance $\bar{R}_{FS}$ is the product of 1) transmission of solar irradiance along ray to scattering volume, 2) forward scattering by volume, and 3) vertical reflection from surface. Surface attenuation radiance $\bar{R}_{SA}$ is the product of 1) transmission of solar irradiance along ray to surface, 2) vertical reflection from surface, and 3) vertical transmission from surface. These radiances can be expressed as

$$\bar{R}_{US} = I_0 \{ C_{S_0} \lambda^{-N} \exp(-X^2/2) [1 - C_A \lambda^{-N} F' - \tfrac{1}{2} C_A \lambda^{-N} \exp(-X^2/2)] \} \tag{8}$$

where $C_{S_0} = \sqrt{2\pi}\, C_0 r_0 A_{s_0}$, $C_A = \sqrt{2\pi}\, C_0 r_0 A_a$, C_0 is the centerline particle concentration, A_{s_0} is the vertical scattering cross section for $\lambda = 1\mu$,

$$F' = \frac{1}{\sqrt{2\pi}} \int_{-\infty}^{+\infty} \exp\left[-\frac{Z^2}{2} - \frac{(X\cos\theta - Z\sin\theta)^2}{2} \right] G_S^{+\infty} \, dZ$$

$X = x/r_0$, $Z = z - z_0/r_0$, $S = X\sin\theta + Z\cos\theta$, and $G_S^{+\infty}$ is the cumulative Gaussian function between $+\infty$ and S (i.e., $G^{+\infty}_{-\infty} = 1$).

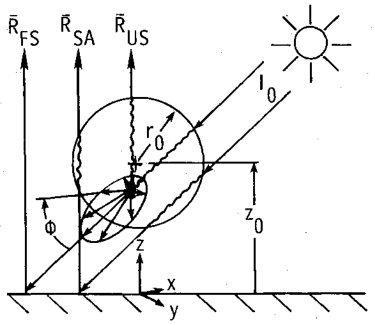

Fig. 5 Components of plume radiance.

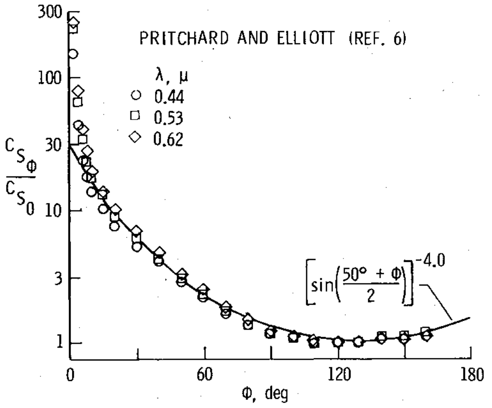

Fig. 6 Empirical scattering function.

$$\bar{R}_{FS} = \bar{R}_{NP} \{ C_{S_0} \lambda^{-N} Z_0 F'' [1 - C_A \lambda^{-N} \exp(-X^2/2)] \} \tag{9}$$

where $\bar{R}_{NP}$ is the scene radiance for the no-plume condition,

$$F'' = \frac{1}{\sqrt{2\pi}\cos\theta} \int_{-\infty}^{+\infty} \left[\frac{\sin(\phi_0 + \phi)}{2} \right]^{-M} (X^2 + Y^2 + Z_0^2)^{-3/2} \, dY$$

where $Y = y/r_0$ and $Z_0 = z_0/r_0$.

$$\bar{R}_{SA} = \bar{R}_{NP} \{ 1 - C_A \lambda^{-N} \exp[-(X\cos\theta + Z_0 \sin\theta)^2/2] - C_A \lambda^{-N} \exp(-X^2/2) \} \tag{10}$$

Several terms require further definition and explanation. The scattering function is related by the empirical expression $[\sin(\phi_0 + \phi)/2]^{-M}$ where ϕ is the scattering angle, M is an empirical constant, and $\phi_0 \approx \theta$. Scattering data[6] are given in Fig. 6 which are in good agreement with the empirical function for $M = 4.0$ and $\phi_0 = 50$ deg. M is a measure of peakedness in the forward scattering, with large values of M being indicative of large particles.

The total (scattering plus absorption) attenuation coefficient C_A can be expressed in terms of the vertical scattering coefficient C_{S_0} in the following manner. Data[7] are presented in Fig. 7 which indicate that the ratio of the total to the scattering attenuation for coal soot particles can be empirically related as

$$C_A / C_{A_s} \approx 1.44\, \lambda^{-0.44}$$

where

$$C_{A_s} = \frac{C_{S_0}}{2} \int_0^\pi \left[\sin\left(\frac{\phi_0 + \phi}{2} \right) \right]^{-M} \sin\phi \, d\phi = \frac{C_{S_0} F'''}{2}$$

Therefore, $C_A = 0.72\, C_{S_0} \lambda^{-0.44} F'''$ can be substituted into Eqs. (8, 9, and 10), eliminating C_A as a determinate.

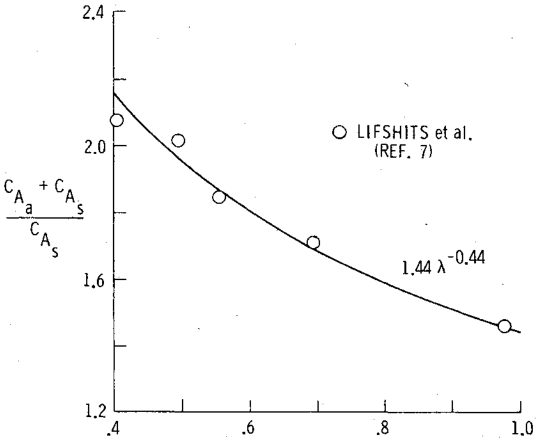

Fig. 7 Absorption-scattering relationship for soot.

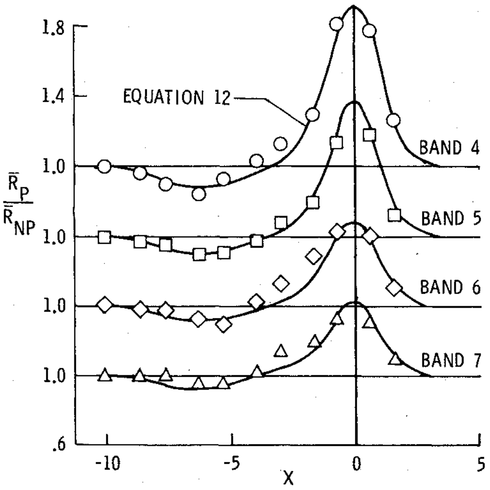

Fig. 8 Radiance profiles, day 2, $L = 1.0$ km.

The three components of plume radiance can be summed giving

$$\bar{R}_P=\bar{R}_{US}+\bar{R}_{FS}+\bar{R}_{SA}=I_0\{\ \}_{US}+\bar{R}_{NP}\{\ \}_{FS}+\bar{R}_{NP}\{\ \}_{SA} \tag{11}$$

(terms within brackets omitted for brevity) which can also be expressed as

$$\bar{R}_P/\bar{R}_{NP}=1/\rho'\{\ \}_{US}+\{\ \}_{FS}+\{\ \}_{SA} \tag{12}$$

where $\bar{R}_{NP}=\rho' I_0$.

Data Results

LANDSAT MSS data analyzed using the present technique were obtained in five strips aligned with the solar azimuth (x direction) as shown in Fig. 2. The data strips were located at distances approximately $L=0.45$, 1.0, 1.8, 2.6, and 3.7 km downwind from the pulp mill stack. Data obtained over the plume on day 1 are the $\bar{R}_P$ (plume) values, while those obtained at the identical (registered) location on day 2 are the $\bar{R}_{NP}$ (no-plume) values, and vice versa. The $\bar{R}_P$ and $\bar{R}_{NP}$ values for all four spectral bands were input into Eq. (11) as a function of their x location along the strip. Plume parameters r_0, z_0, N, M, and C_{S_0} were determined through an iteration procedure by minimizing the root-mean-square (rms) error ϵ between the measured and computed values of $\bar{R}_P$.

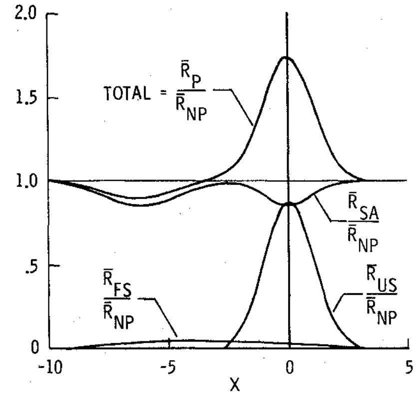

Fig. 9 Components of plume radiance, day 2, $L = 1.0$ km, $\lambda = 0.65\mu$, $\rho' = 0.06$.

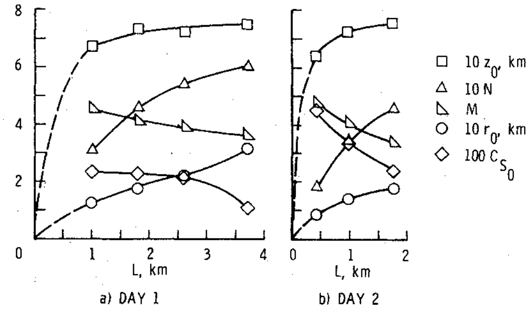

a) DAY 1 b) DAY 2

Fig. 10 Plume parameters for day 1 and day 2.

Measured and computed radiance profiles are presented in Fig. 8 for day 2, $L=1.0$ km. The profiles show a radiance peak at the plume center ($X=0$) and a radiance minimum in the plume shadow (maximum shadow at $X=-Z_0\tan\theta=-6.1$). In Fig. 9, the three components of computed plume radiance are illustrated for band 5 ($\lambda=0.65\mu$). The upward scattered radiance exhibits a characteristic Gaussian distribution about the plume center, while the forward scattered radiance, which is relatively small in the present case, has a maximum value at about $X=-5$. The surface attenuation component exhibits two Gaussian-shaped minimums; one at $X=0$ due to plume attenuation after surface reflection; the other at $X=-6.1$ due to plume attenuation before surface reflection.

Plume parameters computed by the present technique are presented in Fig. 10 for day 1 and 2. Plume radius r_0 exhibits a parabolic growth with distance downwind L, while plume height z_0 increases rapidly during the first kilometer and appears to approach an asymptotic level at about 0.8 km. These are typical characteristics of stack plumes for steady wind conditions.[8] The spectral dependence N and scattering peakedness M also appear to approach asymptotic levels which is indicative of stabilization of the particle size distribution. The scattering coefficient C_{S_0} decreases with distance as the plume diffuses downwind.

Several general comments should be made concerning the plume dynamics and data for day 2. Attempts were made to obtain measurements for the day 2 plume at $L=2.6$ and 3.7 km (see Fig. 2). However, a visual inspection of the measured radiance in the vicinity of $L=2.6$ km indicated that the previously continuous plume had broken into a somewhat circular puff and exhibited two radiance peaks. It was clear that the plume particle distribution could not be considered Gaussian at this location. At the $L=3.7$ km location over the Pamunkey River, the plume was only marginally detectable, either because it had rapidly dispersed or, perhaps, because this data strip was located between puffs. No attempts were made to analyze the data at $L=2.6$ and 3.7 km.

It should not be inferred from the present experience at $L=3.7$ km, day 2, that plumes cannot be detected over water. The entire data strip at $L=0.45$ km, day 2, was located over

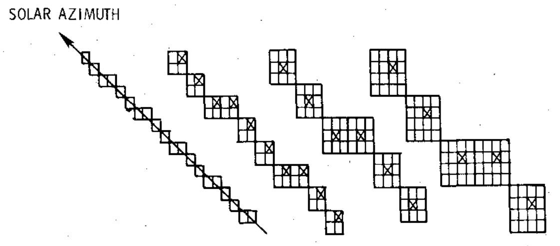

Fig. 11 Alignment and configuration of data pixel sets.

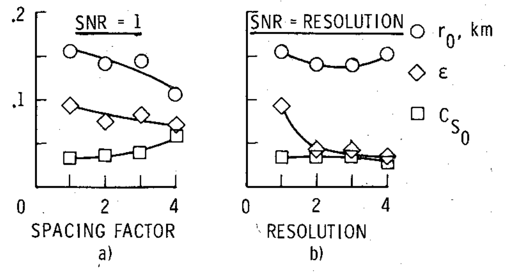

Fig. 12 Spacing factor and resolution, day 2, $L = 1.0$ km.

the Pamunkey River and the plume was easily detected. However, caution should be exerted when analyzing data over dynamic surfaces such as water, because the assumption of little or no surface reflectance change between consecutive days may not be valid.

Physical dimensions of the plume were revealed in Fig. 10, and it is now appropriate to discuss the spatial resolution and signal-to-noise ratio (SNR) of the data strips. The data strips were aligned in the direction of the solar azimuth which was at an angle of about 45 deg to the MSS scan lines. The spatial resolution of the MSS pixel is about 56 m in the scan direction (horizontal) and 79 m along the ground track (vertical). Therefore, as illustrated in Fig. 11, "four-over-three-up" configurations of pixels and pixel sets were used in the present paper in order to have continuous measurements aligned with the solar azimuth.

Statistically, the SNR of the scene measurement is proportional to the square root of the number of individual measurements averaged into the value. If the SNR of a single pixel measurement is normalized to a value of unity, the SNR of averaged 2 by 2, 3 by 3, and 4 by 4 pixel sets would be 2, 3, and 4, respectively. Unfortunately, the normalized spatial resolution of the averaged pixel sets also increases and is equal to the SNR. It is not immediately obvious whether better results would be obtained with low values of both SNR and resolution or high values of both SNR and resolution. Clearly, the size ($\propto r_0$) and the scattering ($\propto C_{S_0}$) of a plume should be the deciding factors.

It is not possible with averaged pixel sets to vary the resolution and SNR independently. However, if a single pixel measurement within a pixel set (crossed pixels in Fig. 11) were chosen to be representative of the set measurement, the measurement would have a normalized SNR of unity and a spacing factor equal to the spatial resolution of the pixel set. In this manner, the effect of SNR can be evaluated at constant values of spacing factor/spatial resolution. It should be recognized that spacing factor and spatial resolution are related, but not truly equivalent terms.

Computed values of plume radius, scattering coefficient, and rms error for day 2, $L = 1.0$ km are given in Figs. 12a and 12b as a function of normalized spacing factor (SNR = 1), and normalized resolution (SNR = resolution), respectively. A comparison of these figures reveals a sharp decrease in ϵ between resolutions of 1 to 2 in Fig. 12b which is clearly due to the increased value of SNR (also from 1 to 2). For further increase in resolution to 3 and 4, the value of ϵ decreases only slightly, which may not be the result of higher SNR, but rather the result of fewer data points (i.e., less data can be better fit). It was concluded from this brief analysis that a normalized resolution and SNR of 2 would probably give the best data results and, therefore, averaged 2 by 2 pixel sets were used for all data. The effective resolution of a 2 by 2 pixel set is about 133 m ($2\sqrt{56 \times 79}$), and the computed plume radius for day 2, $L = 1.0$ km was 139 m. This result suggests that, if the option exists, pixel sets should be chosen that have spatial resolutions approximately equal to the radius of the plume.

One of the major points projected in the present paper is that the no-plume radiance from the surface $\bar{R}_{NP}$ must be known or measured in order to properly evaluate the plume properties. For the present paper, this information was provided by the consecutive-day overpass. An obvious question is, "What results might have been obtained without $\bar{R}_{NP}$ data?" An estimated value of $\bar{R}_{NP}$ can be obtained from $\bar{R}_P$ data taken from locations that are not believed to be influenced by the plume. Such an estimate assumes that the surface reflection directly below the plume is related to that on its boundaries, which may or may not be the case. An average of several $\bar{R}_P$ values taken at locations $-9 > X > 3$ on day 2, $L = 1.0$ km (see Fig. 8) was used as an estimated value of $\bar{R}_{NP}$ in Eq. (11). Computed plume parameters using measured and estimated values of $\bar{R}_{NP}$ can be compared in Table 2. Plume radius, height, and scattering peakedness show no significant changes; however, there are significant changes in the spectral dependence and the $C_{S_0} r_0$ product, both of which are used to compute plume mass loading (discussed in the next section).

The present comparison may be misleading in that it is probably not representative of a typical situation. Measured values of $\bar{R}_{NP}$ were relatively uniform from $X = -10$ to 5 (i.e., farmland), and the average and maximum deviations of the measured values of $\bar{R}_{NP}$ from the estimated mean value of $\bar{R}_{NP}$ were only 6% and 22%, respectively. For most urban industrial areas, it is believed that these deviations would be substantially greater, and the use of estimated $\bar{R}_{NP}$ values could give highly erroneous results.

Only data from two MSS spectral bands are required to compute plume parameters from Eq. (11), and only one band would be required if the spectral dependence of scattering N were known. However, data from all four bands were used to compute all of the results presented in this paper because: 1) there were no theoretical or technical justifications for eliminating any one or more of the bands; and 2) no one or more of the bands, if eliminated, would have consistently reduced the rms error. For example, the rms error ϵ would have been slightly reduced for day 2 if band 7 at $L = 0.45$ km, band 6 at $L = 1.0$ km, and band 4 at $L = 1.8$ km had been eliminated.

Plume parameters were computed for all three- and two-band combinations of data for day 2, $L = 1.0$ km. The results for all three-band combinations and the two-band combination involving bands 4 and 7 were very similar to those obtained using all four bands. However, all other two-band combinations either gave significantly different results, particularly adjacent bands, or their solutions would not

Table 2 Comparison of plume parameters for measured and estimated values of $\bar{R}_{NP}$, day 2, $L = 1.0$ km

	Measured $\bar{R}_{NP}$	Estimated $\bar{R}_{NP}$
r_0, plume radius, km	0.139	0.128
z_0, plume altitude, km	0.725	0.696
N, spectral dependence	0.340	0.401
M, peakedness	4.00	4.17
C_{S_0}, scattering coefficient	0.0331	0.0271
ϵ, rms error	0.0420	0.0594

converge after 100 iterations (four-band computations required seven iterations). General conclusions drawn from these results are: 1) data from all spectral bands available should be incorporated into the results; and 2) if only two bands are available or only two bands are to be used, they should have wide spectral separation.

Estimates of Particle Size Distribution and Mass Loading

The most desired particulate measurements for an industrial stack plume are particle mass loading and diffusion radius. From these measurements, the ground-level concentrations and fallout footprints could be estimated, which are the major environmental goals. An analytical technique for determining the diffusion radius of a stack plume utilizing satellite imagery has been demonstrated in previous sections of this paper. Remote, optical determination of the particle mass loading of a stack plume requires knowledge of the particle size distribution, which can be related through the spectral dependence of particle scattering. However, several studies have shown that when large particles are involved, such as smoke particles, the majority of upward solar scattering comes from particles having radii less than 1μ, while the majority of mass is concentrated in particles having radii greater than 1μ.[9,10] Therefore, it is obvious that any attempts to relate solar scattering measurements to particle mass loading of stack plumes suffer an inherent weakness and require some rather broad assumptions.

There is considerable empirical evidence[10] and a degree of theoretical justification[11] for expressing particle size distribution of aerosols in terms of scattering spectral dependence N as

$$\frac{\mathrm{d}n}{\mathrm{d}r_p} \propto r_p^{\;-(N+3)} \tag{13}$$

where n is the number of particles of radius r_p. If the mean scattering radius of the particles is assumed to be 0.3μ [i.e., $A_{s_0} \approx \pi(0.3\mu)^2$], the plume centerline concentration of these particles can be given as $C_0 \propto C_{S_0}/r_0$ [see discussion of Eq. (8)]. The relationship for concentration of particles of different sizes at different locations is

$$\frac{C_{0_L}}{C_{0_{L_0}}} = \frac{[(r_p/0.3\mu)^{N_{L0}-N_L}]\,(C_{S_0}/r_0)_L}{(C_{S_0}/r_0)_{L0}} \tag{14}$$

The cumulative mass of particles per unit downwind length is given by

$$CM_L \propto \left(\frac{C_{S0}r_0}{1-N}\right)_L \left[\left(\frac{r_p}{0.3\mu}\right)^{1-N} - \left(\frac{r_p}{0.3\mu}\right)^{1-N}_{\min}\right]_L \tag{15}$$

where $r_{p\min.}$ is the minimim-sized particle that contributes significantly to plume mass, assumed here to be 0.1μ. Plume total mass TM_L is determined by evaluating CM_L for $r_p = r_{p\max.}$, assumed here to be 100μ.

Particle number and mass values are given in Fig. 13 for day 1 normalized by the values for $L = 1.0$ km. As expected, the concentration of all particle sizes decreases as the plume diffuses downwind. However, the cumulative mass of midsized particles initially increases, while the mass of larger particles, $r_p > 30\mu$, continuously decreases with downwind location. This behavior is consistent with the following process: 1) coagulation of small particles into midsized particles, 2) coagulation of midsized particles into large particles, and finally, 3) fallout of the large particles.

Emission time $t = L/V$, where V is the wind velocity, is often used as a correlating parameter for plume properties.[8] Plume radius, height, and total mass are presented in Fig. 14 as a function of emission time for day 1 and 2. Plume height, and plume radius to a lesser degree, are well correlated with emission time. Plume total mass appeared to decrease in a somewhat linear manner for the emission time range of the present data; however, it should be expected that these values would asymptotically approach zero values with further increase in time. The particle mass emission rate, which is proportional to the product $TM_0 \times V$, was found to be 20% greater for day 1 than for day 2.

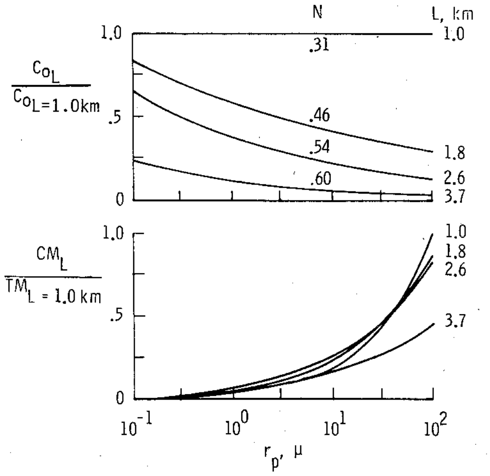

Fig. 13 Particle concentration and mass distribution, day 1.

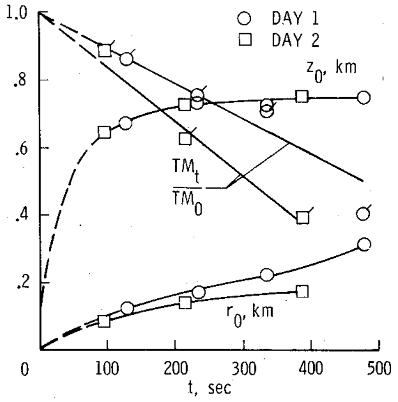

Fig. 14 Comparison of plume parameters.

Observation Opportunities

Remote and ground measurements of smoke particles must be taken for several conditions in order to properly model and access the environmental effects of a smoke-emitting industrial plant. These conditions are meteorological, topographical, and operational in nature and are related through such parameters, for instance, as wind velocity, wind direction, and smoke output. While ground measurements are generally unrestricted in a temporal sense, satellite measurements are limited to orbital site observation opportunities. Major factors which govern these site opportunities are discussed in the following.

Sun Angle

The present plume measurement technique is clearly restricted to daylight opportunities. It is further restricted to solar zenith angles that provide sufficient surface illumination and avoid large atmospheric effects ($\theta < 70$ deg), and to angles that permit the detection of the plume shadow and, hence, plume height ($\theta > 20$ deg). This latter point is illustrated in Fig. 15 where it can be seen that the plume shadow would not have been detectable for $\theta = 10$ deg (simulated effect, day 2, $L = 1.0$ km). Near-noon, sun-synchronous orbits will generally provide acceptable zenith angles and, in addition, minimize both the zenith and azimuth angle differences between plume/no-plume observations.

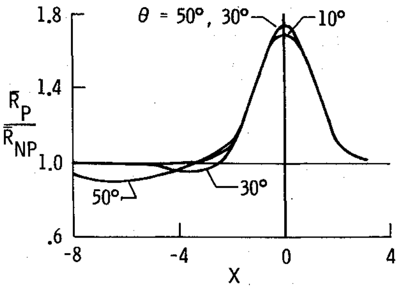

Fig. 15 Simulated zenith angle effect, day 2, $L = 1.0$ km, $\lambda = 0.65\mu$, $\rho' = 0.06$.

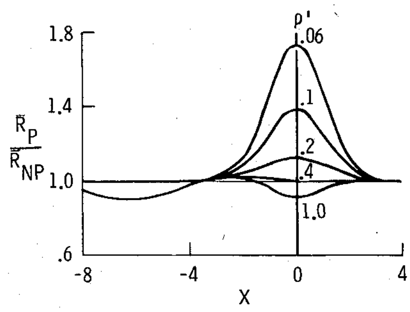

Fig. 16 Simulated surface reflectance effect, day 2, $L = 1.0$ km, $\lambda = 0.65\mu$, $\theta = 50$ deg.

Imagery Overlap

Consecutive-day, overlapping imagery data were used to demonstrate the plume measurement technique in the present paper. However, for the LANDSAT MSS for instance, only one-third of the major industrial plants in the U.S. lie within overlapped regions. While consecutive-day imagery is generally desirable from the data normalization standpoint, the present technique is not restricted to such data.

Repeat Cycle

Both frequent and infrequent orbital repeat cycles offer certain advantages as well as disadvantages. Frequent cycles provide a large number of observations, but for only a small number of sites at acceptably small scan angles, α. Infrequent cycles offer better site coverage at small scan angles, but provide only a small number of observations. It is believed that a 10- to 20-day repeat cycle offers the best compromise between these opposing factors. Clearly, more observation opportunities could be obtained with multiple satellites.

Geostationary orbits offer maximum observation opportunities; however, imagery data obtained from such great distance are not currently of sufficient quality to be of use for monitoring individual stack plumes. In lieu of an advanced imagery system in geostationary orbit, a near-noon, moderate repeat cycle, sun-synchronous orbit similar to the LANDSAT orbit appears to offer the most observation opportunities. The foregoing discussions pertained to potential site opportunities for ideal observation conditions. Meteorological, topographical, and temporal conditions that determine the number of useful opportunities are discussed in the following.

Cloud Cover

Cloud, fog, or haze covers that obstruct plume measurements are a major cause of aborted opportunities. Approximately half of all potential opportunities would be lost for this reason.

Wind Direction

The present plume measurement technique requires the plume flow, and hence wind direction, to be somewhat normal to the solar azimuth. If it is assumed that wind angles up to 45 deg from the azimuth normal are acceptable, approximately half of all potential opportunities would be lost.

Wind Velocity

For some wind velocity conditions, such as no winds, high winds, and/or gusting winds, stack smoke can form smoke clouds or puffs. These smoke formations cannot be analyzed with the present technique.

Surface Reflectance

The normalization procedure requires that no significant surface reflectance changes occur between the plume/no-plume measurements. Snow, ice, or heavy rainfall, for instance, could drastically alter the surface reflectance. Also, as illustrated in Fig. 16 for $\rho' = 0.4$ (simulated effect, day 2, $L = 1.0$ km), certain combinations of surface reflectance and plume concentration would be difficult, if not impossible, to analyze.

Temporal Production

Many industrial plants operate almost continuously on a 24-hour, 7-day-a-week schedule; but most do not. Diurnal, weekly, and seasonal variations of production, and hence smoke, are typical for most plants. Therefore, some opportunities would be lost for these plants during periods of nontypical or no production

All factors considered, it is clear that only a few, perhaps less than 10% of the orbital site observation opportunities would be useful data opportunities. Also, for a number of operational reasons, data would not be taken at every opportunity. Therefore, imagery data must be obtained over relatively long periods in order to have a sufficient data matrix to model the plume dispersions. For instance, LANDSAT I and II have made more than 100 orbital overpasses of every stack site in the U.S., and yet, many of these sites could not be propertly modeled today for lack of sufficient useful data. Even for sites with sufficient data, it is not known how many of these have sufficient ground measurements available to perform a truly comprehensive study of their particulate dispersion patterns. This is a task for future investigations.

Concluding Remarks

LANDSAT I imagery data were analyzed to determine the quantitative properties of a stack plume emitted from a moderate-sized pulp mill. Overlapping, consecutive-day MSS data provided plume/no plume radiances upwelling from the stack site. The data were normalized to correct for atmospheric, solar, and scan angle changes between the two observation days, and cloud shadow data were used to evaluate the atmospheric radiance. Plume radius, height, spectral dependence, scattering coefficient, and phase function were determined at several downwind cross sections. From these parameters, particle size and mass distribution were estimated for the plume.

It is concluded that the LANDSAT sun-synchronous orbit is well suited for sensing stack plume properties. The swath width, spatial resolution, SNR, and spectral bands of the MSS are adequate for determining the particulate properties of large stack plumes. In essence, imagery data that have and will be obtained from the multi-LANDSAT MSS missions meet most of the remote sensing requirements for modeling particulate dispersions in industrial areas.

References

[1] Lyons, W.A. and Pease, S.R., "Detection of Particulate Air Pollution Plumes From Major Point Sources Using ERTS-1 Imagery," *AMS Bulletin,* Vol 54, Nov. 1973, pp. 1163-1170.

[2] Tempelmeyer, K.E. and Ey, D., "Use of Remote Sensing to Study the Dispersion of Stack Plumes," AIAA Paper 75-685, Denver, Colo., May 1975.

[3] Blais, R.N., Copeland, G.E., and Lerner, T.H., "Use of LARS System for the Quantitative Determination of Smoke Plume Lateral

Diffusion Coefficients from ERTS Images of Virginia," *Remote Sensing of Earth Resources,* University of Tennessee Space Institute, Vol. 4, May 1975, pp. 621-633.

[4] *Data Users Handbook*, NASA Goddard Space Flight Center, May 1972, Appendix A, pp. 8-12.

[5] Rogers, R.H. and Peacock, K., "A Technique for Correcting ERTS Data for Solar and Atmospheric Effects," *Symposium on Significant Results Obtained From the Earth Resources Technology Satellite-I,* Vol. I, NASA SP-327, March 1973, pp. 1115-1122.

[6] Pritchard, B.S. and Elliott, W.G., "Two Instruments for Atmospheric Optics Measurements," *Journal of the Optical Society of America,* Vol. 50, March 1960, pp. 191-202.

[7] Lifshits, G.S., Pavlor, V.E., and Milyutin, S.N., "Absorption of Light in Atmospheric Aerosols," *Trudy Astrofizicheskovo in-ta AN Kazakh SSR,* Vol. 7, 1966.

[8] Gifford, F.A., "An Outline of Theories of Diffusion in the Lower Layers of the Atmosphere," *Meteorology and Atomic Energy, 1968,* AEC, July 1968.

[9] Fraser, R.S., "Satellite Measurement of Mass of Sahara Dust in the Atmosphere," *Applied Optics,* Vol. 15, Oct. 1976, pp. 2471-2479.

[10] Laktionov, A.G., "Results of Investigations of Natural Aerosols Over Various Regions of the USSR," *Bulletin of the Academy of Sciences, USSR,* 1960, pp. 373-378.

[11] Volz, F.E., "Optik der Tropfen. I. Optik des Dunstes," *Handbook of Geophysics,* Vol. 8, 1956, pp. 822-897.

From the AIAA Progress in Astronautics and Aeronautics Series...

MATERIALS SCIENCES IN SPACE WITH APPLICATIONS TO SPACE PROCESSING—v. 52

Edited by Leo Steg

The newly acquired ability of man to project scientific instruments into space and to place himself on orbital and lunar spacecraft to spend long periods in extraterrestrial space has brought a vastly enlarged scope to many fields of science and technology. Revolutionary advances have been made as a direct result of our new space technology in astrophysics, ecology, meteorology, communications, resource planning, etc. Another field that may well acquire new dimensions as a result of space technology is that of materials science and materials processing. The environment of space is very much different from that on Earth, a fact that raises the possibility of creating materials with novel properties and perhaps exceptionally valuable uses.

We have had no means for performing trial experiments on Earth that would test the effects of zero gravity for extended durations, of a hard vacuum perhaps one million times harder than the best practical working vacuum attainable on Earth, of a vastly lower level of impurities characteristic of outer space, of sustained extra-atmospheric radiations, and of combinations of these factors. Only now, with large laboratory-style spacecraft, can serious studies be started to explore the challenging field of materials formed in space.

This book is a pioneer collection of papers describing the first efforts in this new and exciting field. They were brought together from several different sources: several meetings held in 1975-76 under the auspices of the American Institute of Aeronautics and Astronautics; an international symposium on space processing of materials held in 1976 by the Committee on Space Research of the International Council of Scientific Unions; and a number of private company reports and specially invited papers. The book is recommended to materials scientists who wish to consider new ideas in a novel laboratory environment and to engineers concerned with advanced technologies of materials processing.

594 pp., 6x9, illus., $20.00 Member $35.00 List

TO ORDER WRITE: Publications Dept., AIAA, 1290 Avenue of the Americas, New York, N.Y. 10019